

Boron Switch for Selectivity of Catalytic Dehydrogenation on Size-Selected Pt Clusters on Al_2O_3

Mai-Anh Ha,^{†,II} Eric T. Baxter,^{‡,II} Ashley C. Cass,[‡] Scott L. Anderson,^{*,‡,ID}
and Anastassia N. Alexandrova^{*,†,§,ID}

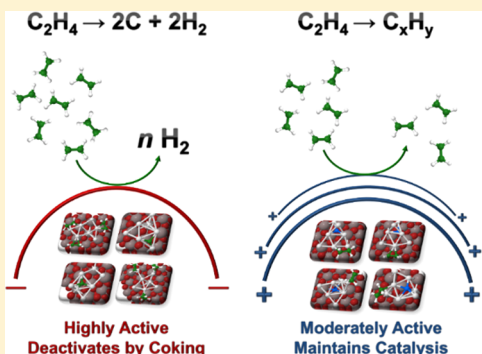
[†]Department of Chemistry & Biochemistry, University of California, Los Angeles, Los Angeles, California 90095, United States

[‡]Department of Chemistry, University of Utah, Salt Lake City, Utah 84112, United States

[§]California NanoSystems Institute, Los Angeles, California 90095, United States

S Supporting Information

ABSTRACT: Size-selected supported clusters of transition metals can be remarkable and highly tunable catalysts. A particular example is Pt clusters deposited on alumina, which have been shown to dehydrogenate hydrocarbons in a size-specific manner. Pt_7 , of the three sizes studied, is the most active and, therefore, like many other catalysts, deactivates by coking during reactions in hydrocarbon-rich environments. Using a combination of experiment and theory, we show that nanoalloying Pt_7 with boron modifies the alkene-binding affinity to reduce coking. From a fundamental perspective, the comparison of experimental and theoretical results shows the importance of considering not simply the most stable cluster isomer, but rather the ensemble of accessible structures as it changes in response to temperature and reagent coverage.



INTRODUCTION

In the subnano-regime of cluster catalysis, size-selected surface-supported clusters often exhibit nonmonotonic trends in reactivity and selectivity, inspiring the hunt for cluster sizes that are particularly active, selective, and resistant to deactivation.^{1–4} Not only can they exhibit special catalytic properties due to size effects on electronic and geometric structure, but also most or all of the atoms in sub-nanoclusters are available to bind reactants, making them a promising and rising class of catalysts. In addition, size-selected clusters provide a theoretically tractable approach to testing strategies for catalyst improvement. We recently showed that Pt_7 deposited on alumina both binds and dehydrogenates ethylene more efficiently than Pt_4 or Pt_8 on either a per cluster or a per Pt atom basis. This higher activity was shown to result from the diverse cluster morphologies accessible to Pt_7 , particularly at higher temperatures and reagent coverages.¹ However, this finding is bittersweet, because these clusters and especially the most active Pt_7 easily deactivate via a combination of coke (i.e., carbon) deposition and sintering. Coke formation deactivates many catalysts in reactions such as Fischer–Tropsch synthesis,⁵ cracking of hydrocarbons,⁶ and alkene dehydrogenation.⁷ Sintering, that is, cluster migration, ripening, and agglomeration into larger nanoparticles, where fewer atoms are available on the surface, is another major route of activity loss.⁸ Thus, improved cluster catalysts would sustain the activity and selectivity of the highly promising Pt_n , while resisting coking and sintering.

In this work, we test the strategy of nanoalloying to tune the selectivity for dehydrogenation by $\text{Pt}_n/\text{Al}_2\text{O}_3$, focusing on Pt_7 , with the goal of minimizing deactivation by coking and sintering. Doping and alloying can be used to tune the properties of bulk Pt. Alloying Pt with Sn⁹ and Zn^{10,11} has been used for selectivity control and with Pd to reduce sintering.^{12,13} Here, our inspiration is drawn from the boration (boron-doping) of extended surfaces of Co and Ni, used in Fischer–Tropsch synthesis and steam methane reforming, respectively.^{14,15} Boration of these metal surfaces extended the lifetime of the catalyst by preventing coke adsorption. In general, boron interacting with metals can lead to a variety of interesting phenomena, such as alloy ultrahardening,¹⁶ emergence of topological and Kondo insulators,¹⁷ exotic magnetism,¹⁸ surface reconstructions,¹⁹ record coordination chemistry,²⁰ and the selectivity of Pd catalysts in hydrogenation.^{21,22} Recently, we began to theoretically probe boron as a dopant for small Pt clusters deposited on magnesia,²³ and found it to reduce affinities of these systems to carbon atoms. Building from this promising initial result, we now address the effect of boration on the selectivity of catalytic dehydrogenation and coking sensitivity of Pt_7 on alumina, using both ab initio and statistical mechanical theory, in conjunction with experiment. In what follows, we show that nanoalloying with boron dramatically changes the properties toward alkene binding and dehydrogenation.

Received: June 7, 2017

Published: July 31, 2017

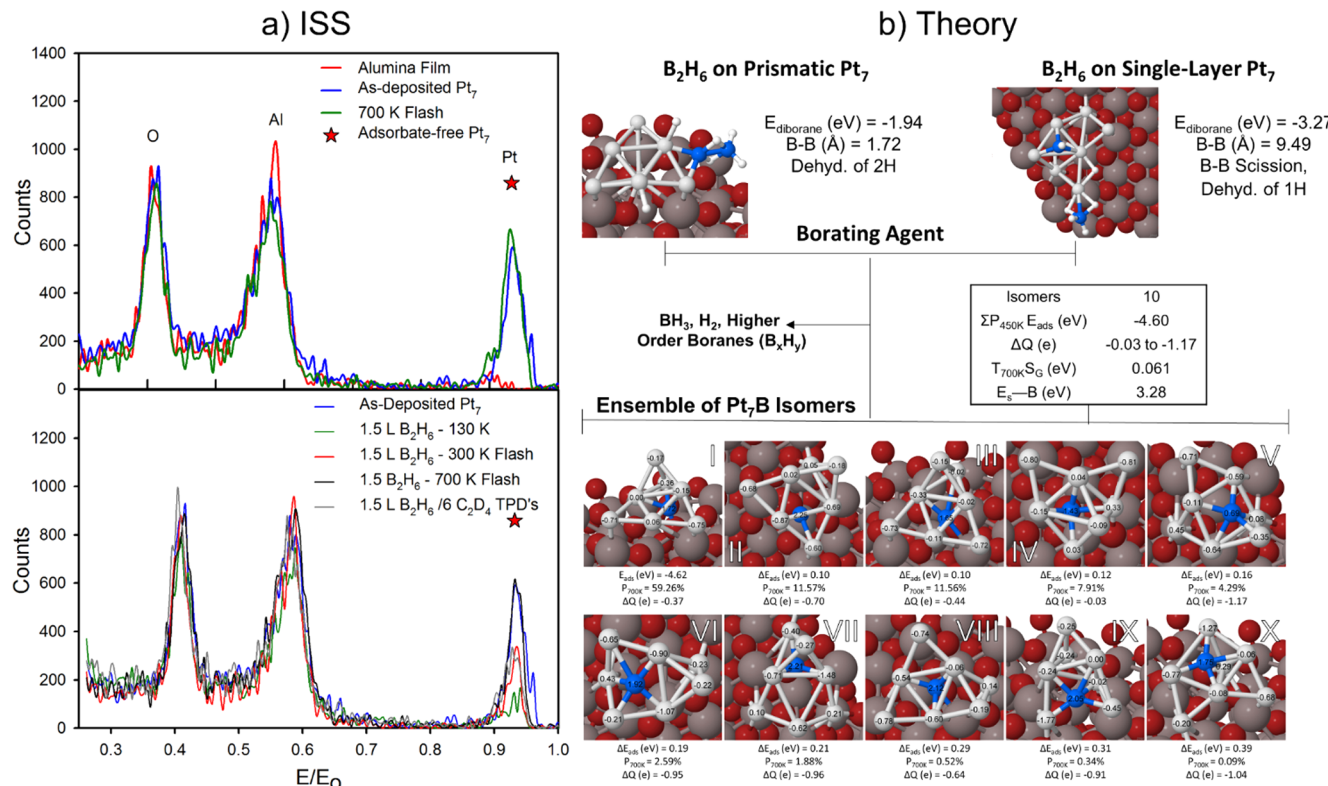


Figure 1. (a) Raw ISS spectra for Pt₇/alumina samples (top) measured immediately after depositing 0.1 ML of Pt₇ (blue) and after flashing Pt₇/alumina to 700 K (green). The spectrum for Pt-free alumina is shown for comparison. (bottom) Raw ISS spectra for as-deposited (blue), after 1.5 L B₂H₆ exposure at 130 K (green), after 1.5 L B₂H₆ at 130 K exposure followed by heating to 300 K (red) or 700 K (black), and after 700 K boration followed by 6 C₂D₄ TPD/R runs (gray). The extrapolated value for adsorbate free Pt₇/alumina is shown by red ★. (b) Diborane adsorption results in borated Pt sub-nanoclusters (top). The lowest minima of adsorbed isomers of Pt₇B with adsorption energy (E_{ads}), adsorption energies of local minima relative to the global minimum (ΔE_{ads}), Boltzmann populations at 700 K, and charge transfer (ΔQ) (bottom). Aluminum atoms are dark gray; oxygen, dark red; platinum, light gray; boron, blue; and hydrogen, white.

RESULTS AND DISCUSSION

Size-selected Pt_{4,7,8} on alumina have been prepared as discussed in detail previously,^{1,24} and then borated by exposure to diborane (B₂H₆). Boration and its effects on binding and dehydrogenation of a model alkene, ethylene, were probed by temperature-programmed desorption/reaction (TPD/R), low energy ion scattering (ISS), plane wave density-functional theory (PW-DFT) calculations, and molecular dynamics (MD) simulations. Initial studies suggested that Pt₇ is not only the most active, but also the most susceptible to the effect of boration. We therefore focused our experimental and theoretical work on Pt₇, and will explore size effects in future studies.

We find that diborane adsorbs dissociatively on the Pt₇ clusters, undergoing both B–H and B–B bond scission, and leaving atoms of boron in the clusters, as it has been reported to do also on the surfaces of Ni,²⁵ Pd,²⁶ Ru,²⁷ Fe or steel,²⁸ Al₂O₃,²⁹ and Pt/Al₂O₃.³⁰ Pt⁰ complexes are also well-known for the successful formation of unique boronated complexes containing borenes, boranes, and borylanes.^{31,32} Notably, Söderlund et al. observed the formation of BH₃, B₃H₇, B₃H₉, B₅H₉, and B₆H₁₀ in fixed bed reactor studies of diborane on Pt/Al₂O₃, and it is likely that this also occurs in our experiments.³⁰ ISS of as-deposited Pt₇/alumina (Figure 1a) shows peaks for O, Al, and Pt. B, itself, is undetectable due to a combination of low ISS sensitivity for B, low B coverage, and high background at low E/E_0 . Nonetheless, because adsorbates attenuate ISS signal

from underlying atoms, the presence of diborane and fragments thereof can be inferred by the effects on other signals.

Considering the Pt signal as reported previously,¹ efficient substrate-mediated adsorption of background CO ($\sim 5 \times 10^{-11}$ mbar) leaves ~ 0.5 CO molecules adsorbed per cluster, on average, and by extrapolation we estimate that the as-deposited Pt signal is $\sim 30\%$ below the adsorbate-free limit (indicated by a ★). Only a small recovery of Pt ISS signal is seen after 700 K heating to desorb adventitious CO, indicating that heating also causes structural changes that result in a smaller fraction of Pt in the surface layer.¹

Initial exposure of a Pt₇/alumina sample to 1.5 L of B₂H₆ at 130 K results in $\sim 80\%$ attenuation of the Pt ISS signal (Figure 1a), demonstrating that diborane binds efficiently on top of Pt₇.^{1,24} Note that 1.5 L exposure may lead to adsorption of more than one diborane per cluster. Because of computational limits, only adsorption of a single diborane adsorbed to Pt₇ clusters was pursued (Figure 1b).

PW-DFT calculations were performed to probe adsorption of a single diborane on Pt₇ isomers. In these 0 K and *in vacuo* calculations, binding of diborane on the prismatic global minimum of Pt₇ results in B–H bond scission with some hydrogen leaving for Pt sites; on the more catalytically active¹ single layer isomer, the B–B bond also breaks with diborane spontaneously decomposing to form BH_y fragments. These results are consistent with the large Pt ISS attenuation observed. The Al and O ISS peaks in ISS underwent only a small attenuation upon diborane exposure at 130 K, indicating

that only a small amount of diborane binds to alumina at 130 K, possibly at defects, and the Al and O peaks largely recover when the sample is heated to 300 K, indicating that most of this initial coverage desorbs at low temperatures.

In the sample heated to 300 K, the Pt signal recovered to ~50% of the as-deposited value, indicating some desorption of diborane or its fragments, but with a significant B_xH_y coverage remaining, attenuating ISS signal from underlying Pt. After heating to 700 K, the Pt signal recovered to the as-deposited value, but was still ~30% below the expected adsorbate-free limit, and also below the signal observed after heating without diborane exposure.

CO TPD (Figure 2) probed the number and energetics of exposed Pt sites. For CO on as-deposited Pt_7 , the main desorption peak is between 300 and 600 K, with a small peak below 200 K. If as-deposited Pt_7 is first simply heated to 700 K in UHV, the total amount of CO desorbing from Pt sites is reduced by ~10%, but the temperature dependence is essentially unchanged. A similar effect is observed if the Pt_7 /alumina is exposed to a saturation dose of D_2 and then heated to 700 K (not shown), consistent with the ISS suggesting thermal restructuring causing a small reduction in the number of exposed Pt sites.

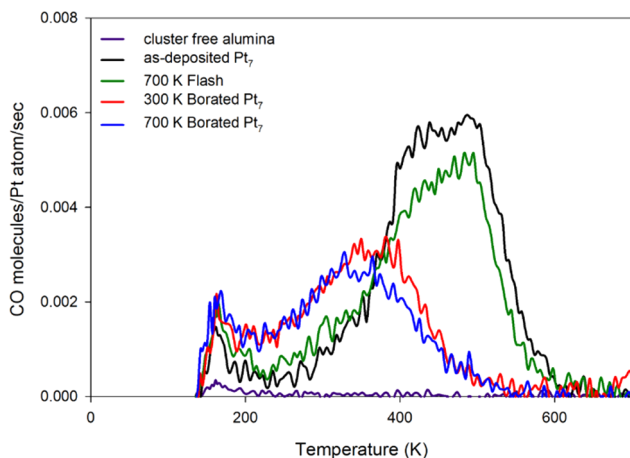


Figure 2. Comparison of CO TPD for a set of Pt_7 /alumina samples that were first exposed to a particular manipulation and then probed by CO TPD (10 L ^{13}CO exposure at 150 K, heating at 3 K/s to 700 K).

Sintering/agglomeration of the Pt_7 into larger clusters, with fewer exposed Pt sites, could potentially account for this small decrease in CO desorption; however, a previous study of CO TPD from Pt_n /alumina/Re(0001) ($2 \leq n \leq 18$)²⁴ found that this CO desorption feature increased significantly with increasing cluster size. Therefore, we conclude that the observed decrease in high-temperature CO desorption after heating cannot be explained by sintering/agglomeration alone. As discussed previously,¹ theory suggests that the ensemble of Pt_7 /isomers favors more prismatic isomers that would also provide fewer CO binding sites.

In any case, it is clear that boration has a much larger effect. For Pt_7 first exposed to 1.5 L of B_2H_6 and heated to 300 K, the CO desorption is attenuated by ~40%, and the main CO desorption peak shifts ~100 K, demonstrating that boration significantly weakens the Pt–CO binding. B_2H_6 exposure followed by 700 K heating has little additional effect on either the number or the energetics of CO binding sites, despite the

observation that 700 K heating results in recovery of the Pt ISS signal to the as-deposited value. The recovery of Pt ISS signal to the as-deposited value following the 700 K heating is further evidence that the observed changes in the CO binding are not a result of thermal sintering.

DFT calculations show that diborane adsorbs dissociatively atop the clusters as fragments of H, B_xH_y , or BH_y (Figure 1b), consistent with the low Pt ISS intensity observed after diborane exposure. However, the majority of Pt_7B/Al_2O_3 structures accessible at 700 K feature the boron acting as a B–O_{surf} anchor between the cluster and the support ($R(\text{B–O}_\text{surf}) \approx 1.4 \text{ \AA}$, isomers I–IV, VII, VIII) with some structures displaying flatter, single-layer geometries with highly coordinated Pt–B bonds (isomers V–VI, IX, X, Figure 1b). All of these structures expose a large fraction of Pt atoms in the surface layer, accounting for high Pt ISS intensity. Pt atoms bonded to B and reduced charge transfer from the support, presumably account for the weakened CO binding. The decomposition of diborane may undergo many pathways,^{33–35} and a future study will elucidate the complex interactions between the borating agent and size-selected clusters.

In our study of nonborated Pt_n /alumina,¹ it was shown that the experimental results were consistent with the theoretical finding of cluster size-dependent ensembles of thermally accessible structures. Predicted evolution of the ensembles with respect to both temperature and ethylene binding was essential to interpreting the ISS and ethylene adsorption results. Because of the increase in complexity of the borated system, such detailed experiment–theory comparison is not feasible; however, theory indicates, perhaps not surprisingly, that Pt_7B /alumina has an even more complex ensemble than Pt_7 /alumina.

In Pt_7B , 10 distinct isomers contribute significantly to the ensemble at 700 K, with the global minimum constituting only 59% of the population. For comparison, the global minimum of Pt_7 on alumina comprised 66% of the ensemble and for the less active Pt_8 , 88%.¹ Thus, the structural diversity unique to Pt_7 /alumina¹ leading to a manifold of binding sites is enhanced in the Pt_7B /alumina ensemble. Having access to diverse isomers introduces the possibility of at least one of them being dominant in catalysis, making the entire ensemble more active, although in more complicated reactions diversity can have an adverse effect on selectivity. At the same time, Pt_7B 's diversity results in a substantial increase in the configurational entropy's contribution to the free energy of the system (Supporting Information, Tables III and IV).¹² These observations are valid only if all thermodynamically accessible isomers are also kinetically accessible.

The effects of boration on ethylene binding and dehydrogenation on Pt_7 were also probed by TPD/R. Figure 3b compares the temperature dependence for C_2D_4 and D_2 desorption from separate Pt_7 /alumina samples, studied as-deposited and after heating to 300 or 700 K, with and without prior 130 K 1.5 L diborane exposure. For as-deposited Pt_7 /alumina, unreacted ethylene desorbs in two components. The low-temperature component is identical to that seen for Pt-free alumina and is attributed to ethylene bound to the alumina support. Desorption from Pt_7 sites occurs in a broad component from ~200 to 500 K. D_2 desorption (dehydrogenation) is not observed for alumina, but appears between ~300 and 650 K for as-deposited Pt_7 /alumina. We previously showed that the onset temperature for D_2 desorption is determined by the activation energy for C_2D_4 dehydrogenation rather than for D_2 desorption.¹ Integrating the desorption signal allows us to

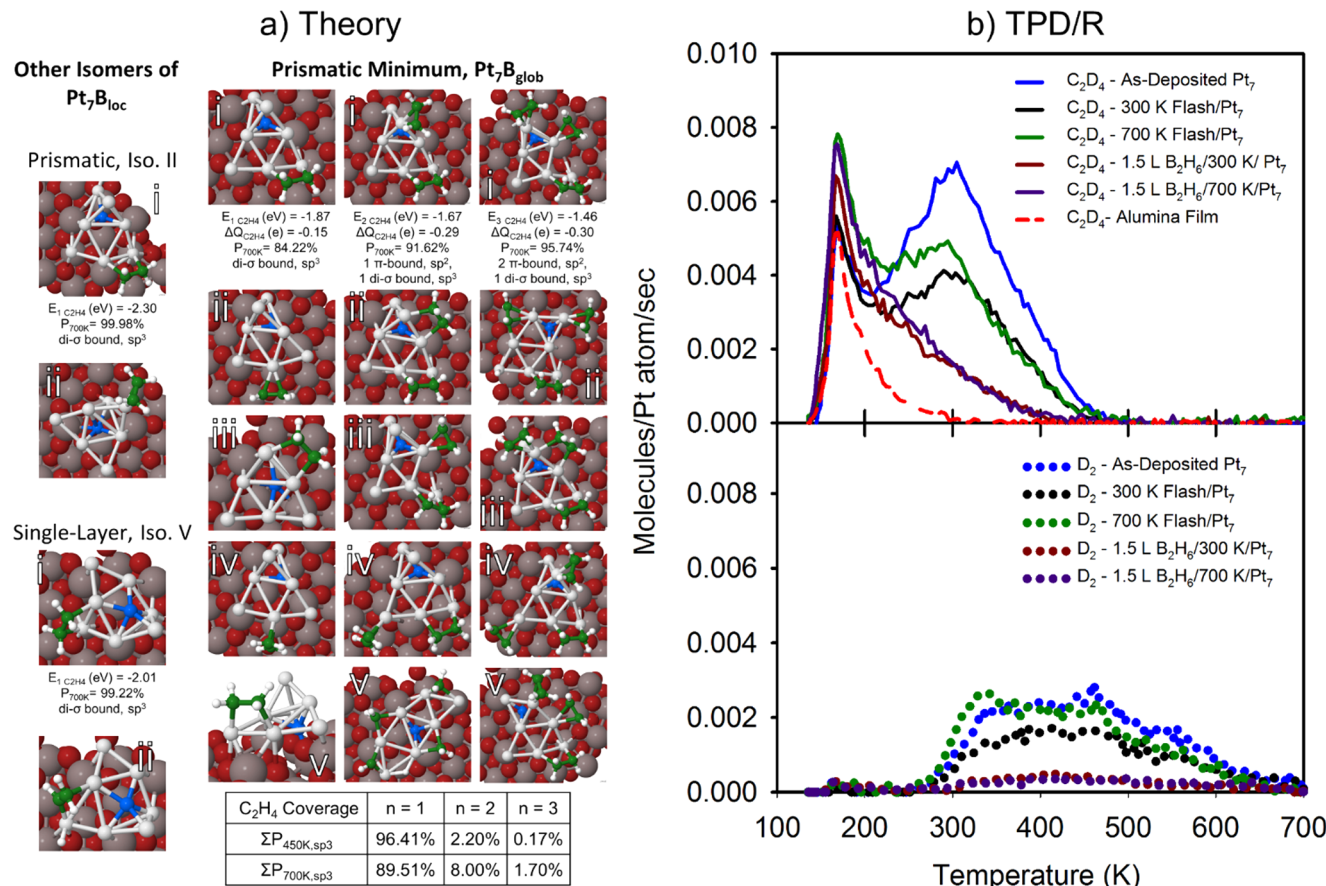


Figure 3. (a) Deposition of ethylene on isomers I, II, and V of Pt_7B from DFT. In π -bound ethylene, both C atoms adsorb to a single Pt site and remain sp^2 -hybridized (bond angles of $\sim 120^\circ$ and a C–C bond-length of $\sim 1.4 \text{ \AA}$). Di- σ bound ethylene binds to two Pt sites and becomes sp^3 -hybridized (bond angles of $\sim 109^\circ$ and a C–C bond of $\sim 1.5 \text{ \AA}$). With increasing temperature and coverage, less ethylene binds as di- σ . Additional minima not visualized here may be found in the [Supporting Information](#) along with other structural data such as charges and bonding discussion. Aluminum atoms are dark gray; oxygen, dark red; platinum, light gray; boron, blue; carbon, green; and hydrogen, white. (b) Intact C_2D_4 (solid) and D_2 (dots) desorbing from Pt_7 /alumina samples after various treatments: as-deposited (blue), 300 K flash (black), 700 K flash (green), 1.5 L of B_2H_6 with 300 K flash (dark red), and 1.5 L of B_2H_6 with 700 K flash (purple). The (red) dashed line represents ethylene desorption from the cluster-free alumina.

estimate the number of C_2D_4 and D_2 molecules desorbing, which, after subtraction of C_2D_4 desorption from alumina, amounts to $\sim 2.1 \text{ C}_2\text{D}_4$ and $\sim 1.5 \text{ D}_2$ molecules per Pt_7 cluster. Assuming that no hydrogen is left on the surface at 700 K,¹ the number of C_2D_4 molecules initially adsorbed is ~ 2.6 per Pt_7 cluster. For as-deposited Pt_7 /alumina heated to 700 K prior to C_2D_4 TPD/R, the amount of C_2D_4 ($\sim 1.8/\text{Pt}_7$) and D_2 ($\sim 1.3/\text{Pt}_7$) is 10–15% lower, and shifted to lower temperatures. The reduction in desorption is stronger if Pt_7 /alumina is heated to only 300 K prior to C_2D_4 TPD/R ($\sim 1.4 \text{ C}_2\text{D}_4$, $\sim 1.0 \text{ D}_2$), presumably because 300 K causes some cluster restructuring, but does not desorb adventitious CO.

Crampton et al. recently reported a study of ethylene hydrogenation to ethane over size-selected Pt_n deposited on MgO that provides an interesting point of comparison.³⁶ In their experiment, they coadsorbed hydrogen and ethylene before carrying out TPR, and measured desorption of ethane. In our experiments, there could potentially also be hydrogen present on the surface due to dissociative adsorption of ethylene; however, we did not see any evidence for ethane production. This absence of ethane production may simply reflect the relatively low concentration of hydrogen, as compared to a situation where hydrogen is dosed along with

ethylene. However, we note that Crampton et al. did not observe hydrogenation for Pt_n smaller than Pt_{10} .

The effects of boration, that is, of 1.5 L diborane exposure and heating, are more dramatic. For either 300 or 700 K heating, desorption of C_2D_4 is strongly attenuated and shifted to lower temperatures (Figure 3b). Note that we do observe a small amount of boron deposition on Pt-free alumina films, presumably at defects; however, this is found to have no effect on the amount or temperature of C_2D_4 desorption. After these contributions are subtracted, the integrated C_2D_4 desorption is found to be only $0.75/\text{Pt}_7$ (300 K) and $0.9/\text{Pt}_7$ (700 K). Boration has no significant effect on the temperature onset for D_2 production, but the amount of D_2 is more than 5 times lower than for as-deposited Pt_7 /alumina (0.27 and $0.25/\text{Pt}_7$ – B_2H_6 for 300 and 700 K heating, respectively). Assuming again that no hydrogen is left on the surface at 700 K, the total initial coverage of ethylene is $\sim 0.83/\text{Pt}_7\text{B}$ and $\sim 1.02/\text{Pt}_7\text{B}$ for samples heated to 300 and 700 K, respectively. It is somewhat surprising that there is not a larger difference between the ethylene chemistry on samples prepared by diborane exposure followed by heating to 300 or 700 K. ISS shows that substantially more B_xH_y adsorbates remain on the surface of the Pt clusters after 300 K heating; yet they appear to have only a modest effect on

the amount of ethylene binding and its propensity to dehydrogenate.

One question is whether any hydrogen is left on the Pt clusters after boration, that is, after diborane exposure and heating to 700 K. If so, this would complicate measurement of ethylene TPD/R because of possible H/D exchange. To test for this process in a somewhat simpler system, we exposed a borated sample to D₂, which adsorbs dissociatively on Pt₇/alumina, undergoing recombinative desorption between ~200 and 350 K. If there were significant H concentration on the sample, significant HD (mass 3) desorption should occur. None was observed, indicating insignificant residual H concentration on the borated samples.

From the perspective of coke reduction, these effects of boration should increase the durability of the catalyst. In alkane dehydrogenation, the goal is to produce alkenes plus hydrogen, but to avoid further dehydrogenation to coke precursors like alkylidenes or alkynes.^{6,9,37,38} It is clear that boration substantially reduces the ethylene adsorption energy to Pt₇, such that desorption occurs below the onset temperature for dehydrogenation (Figure 3b). This constitutes the main result of the present work. Boration tempers but does not kill the catalytic activity of Pt clusters and thus provides a lever for adjusting the selectivity of the catalytic process and a way to eventually optimize it.

DFT provides insight into the mechanism for boron's effects on ethylene binding and decomposition. Pt₇ on alumina is negatively charged from 1.2 to 1.4 e⁻, depending on cluster isomer, due to electron transfer from alumina. Upon boration, the amount of net electron transfer (ΔQ) to the cluster decreases, ranging from nearly neutral -0.3 to -1 e⁻, depending on the isomer. Thus, the nucleophilicity of the Pt₇B/alumina ensemble is substantially reduced as compared to pure Pt₇/alumina. There is charge separation between atoms: positive Pt coordinated to O_{surf}, negative Pt to Al_{surf}, and positive B to O_{surf}; that is, Pt atoms within the clusters are charged nonuniformly. Negative charge is associated with cluster nucleophilicity and strong ethylene binding;¹ thus a substantial reduction in ethylene adsorption energy would be predicted just on the basis of the effects of boron on clusters' charge, consistent with the TPD/R results.

The propensity for coking is governed by how likely ethylene is to desorb from the catalyst rather than undergo dehydrogenation to form coke precursors (CH_y or C_n).^{1,7,37–41} Therefore, we theoretically probed ethylene binding on the ensemble of Pt₇B/alumina structures at relevant temperatures and up to the maximum coverage observed experimentally (~3 ethylene/Pt₇; see Figure 3a). Ethylene binds to Pt in either π - or di- σ -bonded geometries, the latter being associated with further dehydrogenation.^{1,7,37–41} We extracted the structural information for all isomers considered, to construct ensemble percentages of di- σ -bound ethylene as a metric of ethylene activation at rising temperatures and coverages (Figure 3a, see the Supporting Information for details). As noted above, in the experiment, borated Pt₇ binds roughly one ethylene molecule per cluster. DFT shows that ethylene preferentially binds to the more nucleophilic Pt sites on the cluster periphery and avoids the electropositive B (Supporting Information, Figures 4–8, Tables V–VII). Moreover, with increasing coverage, ethylene reflects less cooperative adsorption on Pt₇B than observed on Pt₇: it destabilizes the system by ~0.2 eV/ethylene in Pt₇B, but stabilizes by ~0.3 eV/ethylene in Pt₇.¹

The Pt₇B cluster ensemble also activates a decreasing fraction of ethylene as compared to Pt₇.¹ Pt₇ binds and activates for dehydrogenation more ethylene as the temperature and coverage increase. At 700 K with low coverage, only 15% of Pt₇ isomers contain di- σ ethylene; with high coverage, the percentage increases to >69%. On Pt₇B the effect is the opposite: as the temperature and coverage increase, less additional ethylene bind in the di- σ fashion. This occurs because the population becomes enriched in the species that do not activate ethylene such as the π -configuration. While the first ethylene may bind in the di- σ fashion, all subsequent ethylene molecules prefer the weaker, π -configuration associated with hydrogenation or the desorption observed in experiment. At higher coverage, configurations containing additional sp³, di- σ bound ethylene drop from ~90% to 1.7%. This is the key to the reduced activity of Pt₇B.

Additionally, this illustrates the importance of the ensemble description of cluster catalysts. Note that if we take just the lower limit of temperature and coverage (i.e., consider just global minima with low ethylene content), we would be tempted to conclude that boration promotes rather than suppresses dehydrogenation, based on the prevalence of di- σ -bound ethylene. This result emphasizes that size- and composition-specific properties of surface-deposited cluster catalysts are not just the properties of a single structure, but of the ensembles present under reaction conditions. A number of studies have noted the importance of dynamic fluxionality in the presence of reagents, such as gas-phase Au clusters with CO/H₂O⁴² or H₂,⁴³ H₂S splitting by heterotrimetallic anions,⁴⁴ and supported Au on magnesia⁴⁵ or ceria⁴⁶ for CO oxidation. Our theoretical study provides a comprehensive perspective of ensembles, moving the discussion beyond the low-coverage and low-temperature limit into the realm of real catalysis as evidenced by our discussion and agreement with experiment.

Born–Oppenheimer MD simulations reveal further differences between Pt₇ and Pt₇B interacting with ethylene (Supporting Information, Figures 9–13). In a previous publication, we predicted that in pure Pt₇ clusters, prismatic geometries would stabilize to single-layer geometries during ethylene adsorption.¹ We observe this in MD trajectories at 450, 700, and 1000 K (Supporting Information, Figure 9). At 450 and 700 K, the prismatic geometry undergoes multiple transformations: it opens from a prism to a distorted hexagon (circa MD step 150) and varies between other prismatic configurations and other single-layer configurations. At 1000 K, ethylene adsorbed to either the prismatic or the single-layer Pt₇ converts to the di- σ configuration. On single-layer Pt₇, ethylene exhibits C–H bond activation, followed by H₂ formation (Supporting Information, Figure 10). These MD trajectories demonstrate the high reactivity of single-layer structures, particularly, in pure Pt₇.

We considered Pt₇B isomers I, II, and V as representatives of different structural classes. At 450 and 700 K with one bound ethylene molecule, the prismatic isomers I and II undergo flattening into single-layer and extended, branched configurations around the B–O_{surf} anchor, exhibiting high fluxionality. At 700 K, the strongly bound, di- σ ethylene either desorbs (on isomer I) or interconverts to π -bound (on isomer II), i.e., reverts to a geometry where it should tend to hydrogenate or desorb. On the single-layer isomer V of Pt₇B, we observe activation of the C–C and C–H bonds. At 450 K, we see the activation of the C–H bonds proceeding to dissociation of 2H. At 700 K, minor restructuring of the single-layer cluster isomer

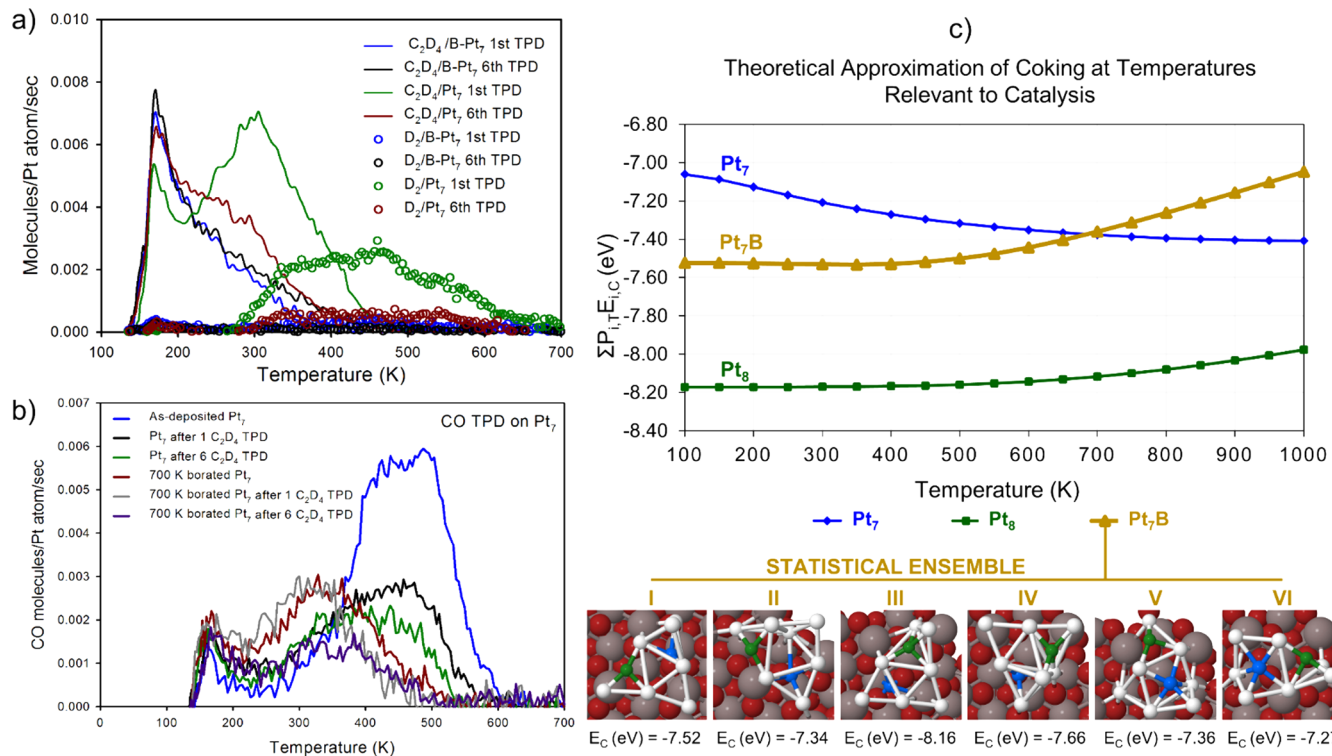


Figure 4. (a) Intact C₂D₄ (solid) and D₂ (dots) desorbing from Pt₇/alumina samples after various treatments: Pt₇ 1st TPD/R run (green), Pt₇ 6th C₂D₄ TPD/R run (dark red), borated Pt₇ 1st TPD/R run (blue), and borated Pt₇ 6th TPD/R run (black). (b) CO TPD from Pt₇ with different treatments: Pt₇ as-deposited (blue), Pt₇ after one C₂D₄ TPD/R run (black), Pt₇ after six C₂D₄ TPD/R runs (green), borated Pt₇ as prepared (dark red), borated Pt₇ after one C₂D₄ TPD/R run (gray), and borated Pt₇ after six C₂D₄ TPD/R runs (purple). The number of CO binding sites on pure Pt₇/alumina dramatically decreases after dehydrogenation, whereas borated clusters show fewer CO binding sites and shift toward weaker CO binding. (c) First-order approximation of coking: Boltzmann-weighted C-sticking energies for an ensemble. The Pt₇B isomers included in the ensemble are visualized at the bottom. As temperature rises, borated Pt exhibits increasing resistance to carbon. Boltzmann weights utilized as-deposited Pt₇, Pt₈, and Pt₇B adsorption energies. Aluminum atoms are dark gray; oxygen, dark red; platinum, light gray; boron, blue; and carbon, green.

occurs, and the di- σ -bound ethylene converts to π -bound. Dehydrogenation appears to proceed through a transition of an H atom from C to a neighboring Pt atom. Born–Oppenheimer MD shows that a vast variety of structures of Pt₇B with bound ethylene are dynamically visited at temperatures of 450 and 700 K (see Supporting Information, Figures 11–13). Even though these MD trajectories give only a partial view on the kinetic accessibility of the isomers, the results of dynamics simulations support the high isomeric diversity and the ensemble description used throughout this study. Thus, MD of these representative Pt₇B isomers available for catalysis supports the reduced activity of borated Pt₇ as compared to pure Pt₇.

Evidence that boration stabilized the catalyst is provided by monitoring changes during 6 sequential TPD/R runs (Figure 4a). For Pt₇/alumina, the amounts of both C₂D₄ and D₂ desorbing decrease substantially, and post-reaction XPS shows significant carbon deposition.¹ For borated Pt₇/alumina, there is essentially no change in C₂D₄ and D₂ desorption and no XPS-detectable carbon deposition. Indeed, boration lowers the C₂D₄ binding energy such that desorption, rather than dehydrogenation and coking, is favored.

The CO TPD in Figure 4b reveals additional details. For pure Pt₇, the number of CO binding sites is reduced dramatically after 1 C₂D₄ TPD/R run, and continues to drop during 6 C₂D₄ TPD/R runs, exhibiting binding site loss from some combination of coke deposition and cluster sintering/restructuring. Borated clusters also show a gradual decrease in

the number of CO sites from sequential C₂D₄ TPD/R runs. Because no C deposits are detected with XPS, we conclude that the effect is likely attributable to cluster sintering, as supported by the smaller calculated binding energies of Pt₇B to the support (Supporting Information, Tables III and IV) and greater fluxionality of shapes seen in MD, as compared to Pt₇.

Finally, we consider coking in terms of the affinity of the clusters to C atoms. As a first-order approximation, we analyzed the Boltzmann-weighted ensemble-averages of the C-binding energies (E_C) of the isomers that constitute >96% of the population at 450 and 700 K, for Pt₇, Pt₇B, and Pt₈ (Figure 4c), the latter included because it tends to have prismatic isomers like Pt₇B. Carbon affinity is both temperature- and isomer-dependent, but the temperature dependence for Pt₇ and Pt₇B is opposite. For Pt₇, the ensemble-average E_C increases with temperature; that is, the population evolves to include more isomers with high carbon affinity. In contrast, for Pt₇B, higher-energy planar configurations (isomers V and VI) in which B is exposed, rather than anchored to alumina (isomers I–IV), exhibit weaker E_C . As a result, the evolving ensemble for Pt₇B has decreasing carbon affinity and therefore increasing coke-resistance as temperature rises. For Pt₈, E_C also decreases with temperature, but remains much higher than for Pt₇B. Pt₇B's resistance to carbon can again be traced to its reduced negative charge and nucleophilicity.

CONCLUSION

We show that nanoalloying of small, alumina-supported Pt clusters with boron has a substantial effect on the selectivity of catalytic dehydrogenation of ethylene. Boration reduces the ethylene binding energy and thus the tendency toward undesired dehydrogenation to coke precursors. Coking is one of the major mechanisms for cluster catalyst deactivation, and therefore the proposed strategy of its mitigation might be broadly valuable. The effect is linked to cluster morphologies in the statistical ensemble accessible at experimental conditions of temperature and ethylene coverage. As both temperature and coverage increase, borated clusters activate less ethylene for dehydrogenation and bind less carbon more weakly, as an ensemble, while the opposite is true for pure Pt clusters. Fundamentally, this work illustrates how size- and composition-specific properties of cluster catalysts are necessarily ensemble-averages and cannot be described by individual structures, even if they are the global minima.

METHODS

Experimental Section. The experimental protocol has been detailed elsewhere.¹ Briefly, experiments were performed using an instrument that allows *in situ* sample preparation by cluster deposition and characterization by a variety of methods. Pt₇/alumina samples were prepared in ultrahigh vacuum ($\sim 1.5 \times 10^{-10}$ Torr) by growing an alumina thin film (~ 3 nm) on a Ta(110) single crystal, and soft landing (1 eV/atom) mass-selected Pt₇ clusters onto the support. The alumina thin films were grown using procedures adapted from the work of the Goodman^{47–49} and Maday^{50,51} groups. A detailed study by Chen and Goodman⁴⁷ concluded that alumina thin (~ 1.5 Å) films grown on a Ta(110) single crystal have slightly distorted hexagonal symmetry that can be related to either the (0001) face of $\alpha\text{-Al}_2\text{O}_3$ or the (111) face of $\gamma\text{-Al}_2\text{O}_3$. Because the films were inert to a variety of gas molecules under vacuum, the films were proposed to be preferentially oxygen terminated.^{52,53} In previous publications,^{52,53} we demonstrated that the adsorbate binding, reactivity, and electronic properties of Pd clusters deposited on these alumina thin films were independent of film thickness in the 3–10 nm range. In the present study, we used 3–6 nm thick films. Cluster coverage was controlled by monitoring the cluster neutralization current. All samples contained Pt₇ coverage corresponding to 1.5×10^{14} atoms/cm² (~ 0.1 Pt monolayer). Deposition took ~ 5 –15 min.

TPD/R measurements were made with a differentially pumped mass spectrometer that views the sample through a ~ 2.5 mm diameter orifice in a skimmer cone, which is surrounded by directional dose tubes allowing gas exposures to the sample. For the ethylene TPD/R measurement, the sample was exposed to 5 L of C₂D₄ at a sample temperature of 150 K. The sample was then cooled to 135 K and ramped to 700 at 3 K/s, while monitoring masses of interest desorbing from the surface. For CO TPD, samples were exposed to 10 L of ¹³C¹⁶O at a sample temperature of 150 K, cooled to 135 K, and ramped to 700 at 3 K/s, while monitoring desorption of ¹³CO and other masses of interest. Boration was done by exposing samples to 1.5 L of B₂H₆ at a sample temperature of 130 K, and then ramping the sample temperature up to either 300 or 700 at 3 K/s. Note that all experiments were carried out on separately prepared samples to avoid thermal or adsorbate-induced changes to the samples.

Low energy He⁺ ion scattering spectroscopy (1 keV He⁺, 45° angle of incidence, normal detection) was used to observe the effects of cluster size, sample heating, boration, and ethylene TPD/R on the fraction of Pt atoms exposed in the surface layer. ISS peaks result from He⁺ scattering from single atoms in the surface layer, identifying the masses of those atoms. Because ISS is a destructive technique, all measurements were made on separately prepared samples or at the end of a series of experimental sequences.

Computational. As discussed previously,¹ PW-DFT calculations were performed using the Vienna Ab initio Simulation Package

(VASP)^{54–57} utilizing projector augmented wave potentials^{58,59} and the PBE⁶⁰ functional. A dense Monkhorst–Pack $8 \times 8 \times 3$ k-point grid was implemented for bulk calculations of the $\alpha\text{-Al}_2\text{O}_3$ unit cell with large kinetic energy cutoffs of 520.0 eV. The optimized lattice constants of $a = 4.807$ Å and $c = 13.126$ Å exhibited a slight increase of <0.1 Å as compared to experiment, typical of GGA functionals.^{61,62} The unit cell was grown to a (3 \times 3) surface with the bottom half of the surface kept fixed and a vacuum gap of 15 Å. A 1 \times 1 \times 1 k-point grid centered at Γ -point, stringent convergence criteria of 10^{-5} (10^{-6}) eV for geometric (electronic) relaxations, and kinetic energy cutoffs of 400.0 eV were employed in all calculations. The Adaptive Force Field Coalescence Kick (AFFCK),⁶³ an adaptive global minimum and local minima search based on the Coalescence Kick (CK),⁶⁴ was used to find gas-phase Pt₇B. A per manum search of adsorbed structures consisted of deposition of the lowest 5–6 gas-phase structures (Supporting Information, Figure 1) under PBE levels of theory with a thorough sampling of cluster faces to possible binding sites. It must be noted that with larger gas-phase clusters, the order of the lowest minima may be DFT method dependent.⁶³ All relevant equations such as the adsorption of reagents, sintering penalty, Gibbs or configurational entropy, among others, may be found in the Supporting Information. MD calculations were also performed in VASP requiring electronic iterations to reach a convergence criterion of 10^{-8} eV per 1 fs time-step. MD trajectories of >1.5 ps were analyzed to compare adsorption behavior of ethylene on pure Pt versus borated Pt. The Nose–Hoover thermostat was used to equilibrate the system, approximating conditions to that of the NVT ensemble.

ASSOCIATED CONTENT

Supporting Information

The Supporting Information is available free of charge on the ACS Publications website at DOI: 10.1021/jacs.7b05894.

Experimental and theoretical data (PDF)

AUTHOR INFORMATION

Corresponding Authors

*anderson@chem.utah.edu
*ana@chem.ucla.edu

ORCID

Scott L. Anderson: 0000-0001-9985-8178
Anastassia N. Alexandrova: 0000-0002-3003-1911

Author Contributions

[†]M.-A.H. and E.T.B. contributed equally to this work.

Notes

The authors declare no competing financial interest.

ACKNOWLEDGMENTS

This work was supported by the Air Force Office of Scientific Research under a Basic Research Initiative grant (AFOSR FA9550-16-1-0141) to A.N.A. and S.L.A. M.-A.H. was also funded by the UCLA Graduate Division Dissertation Year Fellowship. CPU resources at the DoD (Department of Defense) High Performance Computing Modernization Program (the U.S. Air Force Research Laboratory DoD Supercomputing Resource Center—AFRL DSRC, the U.S. Army Engineer Research and Development Center—ERDC, and the Navy Supercomputing Resource Center—Navy DSRC), Pacific Northwest National Laboratory’s Environmental Molecular Sciences Laboratory’s (EMSL) Cascade cluster, Extreme Science and Engineering Discovery Environment’s (XSEDE) computing resources, and the UCLA-IDRE cluster were used to conduct this work.

■ REFERENCES

- (1) Baxter, E. T.; Ha, M.; Cass, A. C.; Alexandrova, A. N.; Anderson, S. L. *ACS Catal.* **2017**, *7*, 3322–3335.
- (2) Kaden, W. E.; Wu, T.; Kunkel, W. A.; Anderson, S. L. *Science* **2009**, *326*, 826–829.
- (3) Vajda, S.; Pellin, M. J.; Greeley, J. P.; Marshall, C. L.; Curtiss, L. A.; Ballentine, G. A.; Elam, J. W.; Catillon-Mucherrie, S.; Redfern, P. C.; Mahmood, F. *Nat. Mater.* **2009**, *8*, 213–216.
- (4) Lee, S.; Molina, L. M.; López, M. J.; Alonso, J. A.; Hammer, B.; Lee, B.; Seifert, S.; Winans, R. E.; Elam, J. W.; Pellin, M. J. *Angew. Chem.* **2009**, *121*, 1495–1499.
- (5) Schulz, H. *Appl. Catal., A* **1999**, *186*, 3–12.
- (6) Rahimi, N.; Karimzadeh, R. *Appl. Catal., A* **2011**, *398*, 1–17.
- (7) Shaikhutdinov, S. K.; Frank, M.; Bäumer, M.; Jackson, S. D.; Oldman, R. J.; Hemminger, J. C.; Freund, H. *Catal. Lett.* **2002**, *80*, 115–122.
- (8) Hansen, T. W.; DeLaRiva, A. T.; Challa, S. R.; Datye, A. K. *Acc. Chem. Res.* **2013**, *46*, 1720–1730.
- (9) Galvita, V.; Siddiqi, G.; Sun, P.; Bell, A. T. *J. Catal.* **2010**, *271*, 209–219.
- (10) Dadras, J.; Shen, L.; Alexandrova, A. N. *J. Phys. Chem. C* **2015**, *119*, 6047–6055.
- (11) Shen, L.; Dadras, J.; Alexandrova, A. N. *Phys. Chem. Chem. Phys.* **2014**, *16*, 26436–26442.
- (12) Ha, M.; Dadras, J.; Alexandrova, A. N. *ACS Catal.* **2014**, *4*, 3570–3580.
- (13) Johns, T. R.; Gaudet, J. R.; Peterson, E. J.; Miller, J. T.; Stach, E. A.; Kim, C. H.; Balogh, M. P.; Datye, A. K. *ChemCatChem* **2013**, *5*, 2636–2645.
- (14) Tan, K. F.; Chang, J.; Borgna, A.; Saeys, M. *J. Catal.* **2011**, *280*, 50–59.
- (15) Xu, J.; Chen, L.; Tan, K. F.; Borgna, A.; Saeys, M. *J. Catal.* **2009**, *261*, 158–165.
- (16) Levine, J. B.; Tolbert, S. H.; Kaner, R. B. *Adv. Funct. Mater.* **2009**, *19*, 3519–3533.
- (17) Cooley, J.; Aronson, M.; Fisk, Z.; Canfield, P. *Phys. Rev. Lett.* **1995**, *74*, 1629.
- (18) KüPers, M.; Lutz-Kappelman, L.; Zhang, Y.; Miller, G. J.; Fokwa, B. P. *Inorg. Chem.* **2016**, *55*, 5640–5648.
- (19) Nandula, A.; Trinh, Q. T.; Saeys, M.; Alexandrova, A. N. *Angew. Chem., Int. Ed.* **2015**, *54*, 5312–5316.
- (20) Popov, I. A.; Jian, T.; Lopez, G. V.; Boldyrev, A. I.; Wang, L. S. *Nat. Commun.* **2015**, *6*, 8654.
- (21) Chan, C. W. A.; Mahadi, A. H.; Li, M. M.; Corbos, E. C.; Tang, C.; Jones, G.; Kuo, W. C. H.; Cookson, J.; Brown, C. M.; Bishop, P. T. *Nat. Commun.* **2014**, *5*, 5787.
- (22) Krawczyk, M.; Sobczak, J.; Palczewska, W. *Catal. Lett.* **1993**, *17*, 21–28.
- (23) Dadras, J.; Jimenez-Izal, E.; Alexandrova, A. N. *ACS Catal.* **2015**, *5*, 5719–5727.
- (24) Roberts, F. S.; Kane, M. D.; Baxter, E. T.; Anderson, S. L. *Phys. Chem. Chem. Phys.* **2014**, *16*, 26443–26457.
- (25) Desrosiers, R. M.; Greve, D. W.; Gellman, A. J. *J. Vac. Sci. Technol., A* **1997**, *15*, 2181–2189.
- (26) Krawczyk, M. *Appl. Surf. Sci.* **1998**, *135*, 209–217.
- (27) Rodriguez, J. A.; Truong, C. M.; Corneille, J.; Goodman, D. W. *J. Phys. Chem.* **1992**, *96*, 334–341.
- (28) Casadesus, P.; Frantz, C.; Gantois, M. *Metall. Trans. A* **1979**, *10*, 1739–1743.
- (29) Weiss, H.; Knight, J.; Shapiro, I. *J. Am. Chem. Soc.* **1959**, *81*, 1826–1827.
- (30) Söderlund, M.; Mäki-Arvela, P.; Eränen, K.; Salmi, T.; Rahkola, R.; Murzin, D. Y. *Catal. Lett.* **2005**, *105*, 191–202.
- (31) Arnold, N.; Braunschweig, H.; Dewhurst, R. D.; Ewing, W. C. *J. Am. Chem. Soc.* **2016**, *138*, 76–79.
- (32) Cui, Q.; Musaev, D. G.; Morokuma, K. *Organometallics* **1998**, *17*, 742–751.
- (33) McKee, M. L. *J. Phys. Chem.* **1990**, *94*, 435–440.
- (34) Curtiss, L. A.; Pople, J. A. *J. Chem. Phys.* **1989**, *90*, 2522–2523.
- (35) Ganguli, P.; McGee, H., Jr. *J. Chem. Phys.* **1969**, *50*, 4658–4660.
- (36) Crampton, A. S.; Rötzer, M. D.; Ridge, C. J.; Schweinberger, F. F.; Heiz, U.; Yoon, B.; Landman, U. *Nat. Commun.* **2016**, *7*, 10389.
- (37) Neurock, M.; van Santen, R. A. *J. Phys. Chem. B* **2000**, *104*, 11127–11145.
- (38) Chen, Y.; Vlachos, D. G. *J. Phys. Chem. C* **2010**, *114*, 4973–4982.
- (39) Anderson, A. B.; Choe, S. *J. Phys. Chem.* **1989**, *93*, 6145–6149.
- (40) Windham, R. G.; Koel, B. E. *J. Phys. Chem.* **1990**, *94*, 1489–1496.
- (41) Windham, R.; Koel, B. E.; Paffett, M. *Langmuir* **1988**, *4*, 1113–1118.
- (42) Xing, X.; Li, X.; Yoon, B.; Landman, U.; Parks, J. H. *Int. J. Mass Spectrom.* **2015**, *377*, 393–402.
- (43) Gao, M.; Lyalin, A.; Takagi, M.; Maeda, S.; Taketsugu, T. *J. Phys. Chem. C* **2015**, *119*, 11120–11130.
- (44) Adhikari, D.; Raghavachari, K. *J. Phys. Chem. A* **2016**, *120*, 466–472.
- (45) Häkkinen, H.; Abbet, S.; Sanchez, A.; Heiz, U.; Landman, U. *Angew. Chem., Int. Ed.* **2003**, *42*, 1297–1300.
- (46) Ghosh, P.; Farnesi Camellone, M.; Fabris, S. *J. Phys. Chem. Lett.* **2013**, *4*, 2256–2263.
- (47) Chen, P.; Goodman, D. *Surf. Sci.* **1994**, *312*, L767–L773.
- (48) Street, S.; Goodman, D.; King, D.; Woodruff, D. *Chem. Phys. Solid Surf.* **1997**, *8*, 375–406.
- (49) Lai, X.; Chusuei, C. C.; Luo, K.; Guo, Q.; Goodman, D. *Chem. Phys. Lett.* **2000**, *330*, 226–230.
- (50) Wu, Y.; Garfunkel, E.; Madey, T. E. *Surf. Sci.* **1996**, *365*, 337–352.
- (51) Wu, Y.; Garfunkel, E.; Madey, T. E. *J. Vac. Sci. Technol., A* **1996**, *14*, 2554–2563.
- (52) Kane, M. D.; Roberts, F. S.; Anderson, S. L. *Faraday Discuss.* **2013**, *162*, 323–340.
- (53) Kane, M. D.; Roberts, F. S.; Anderson, S. L. *J. Phys. Chem. C* **2015**, *119*, 1359–1375.
- (54) Kresse, G.; Hafner, J. *Phys. Rev. B: Condens. Matter Mater. Phys.* **1993**, *47*, 558.
- (55) Kresse, G.; Hafner, J. *Phys. Rev. B: Condens. Matter Mater. Phys.* **1994**, *49*, 14251.
- (56) Kresse, G.; Furthmüller, J. *Comput. Mater. Sci.* **1996**, *6*, 15–50.
- (57) Kresse, G.; Furthmüller, J. *Phys. Rev. B: Condens. Matter Mater. Phys.* **1996**, *54*, 11169.
- (58) Blöchl, P. E. *Phys. Rev. B: Condens. Matter Mater. Phys.* **1994**, *50*, 17953.
- (59) Kresse, G.; Joubert, D. *Phys. Rev. B: Condens. Matter Mater. Phys.* **1999**, *59*, 1758.
- (60) Perdew, J. P.; Burke, K.; Ernzerhof, M. *Phys. Rev. Lett.* **1996**, *77*, 3865.
- (61) Bourdillon, A.; El-Mashri, S.; Forty, A. *Philos. Mag. A* **1984**, *49*, 341–352.
- (62) Levin, I.; Brandon, D. *J. Am. Ceram. Soc.* **1998**, *81*, 1995–2012.
- (63) Zhai, H.; Ha, M.; Alexandrova, A. N. *J. Chem. Theory Comput.* **2015**, *11*, 2385–2393.
- (64) Averkiev, B. Ph.D. Thesis, Utah State University, Logan, UT, 2009.